Thermal modeling of gain competition in Yb-doped large-mode-area photonic-crystal fiber amplifier

Lorenzo Rosa,[1,2,*] **Enrico Coscelli,**[1] **Federica Poli,**[1] **Annamaria Cucinotta,**[1] **and Stefano Selleri**[1]

[1]*Dept. Information Engineering, University of Parma, V. Usberti 181/A, I-43124 Parma, Italy*
[2]*Applied Plasmonics, Centre for Micro-Photonics, Swinburne University of Technology, P.O.Box 218, Hawthorn, VIC 3122, Australia*
[*]*LRosa@ieee.org*

Abstract: We propose a new model for gain competition effects in high-power fiber amplifiers, which accounts for the thermal effects of heat load on the doped core overlap of the propagating light field. The full-vectorial nature of the fiber modes is modeled by an embedded finite-element method modal solver, and the temperature profile is calculated by a simple and efficient radial heat propagation solver. The model is applied to a Yb^{3+}-doped LPF45 air-clad photonic-crystal fiber amplifier for co- and counter-propagating pumping setups, showing gain competition in conditions of severe heat load.

OCIS codes: (060.2320) Fiber optics amplifiers and oscillators; (060.5295) Photonic crystal fibers; (140.6810) Thermal effects.

References and links

1. A. Tünnermann, T. Schreiber, and J. Limpert, "Fiber lasers and amplifiers: an ultrafast performance evolution," Appl. Opt. **49**, F71–F78 (2010).
2. D. J. Richardson, J. Nilsson, and W. A. Clarkson, "High power fiber lasers: current status and future perspectives," J. Opt. Soc. Am. B **27**, B63–B92 (2010).
3. M. N. Zervas, C. A. Codemard, "High power fiber lasers: a review," IEEE J. Sel. Top. Quantum Electron. **20**(5), 0904123 (2014).
4. F. Poli, A. Cucinotta, and S. Selleri, *Photonic Crystal Fibers. Properties and Applications*, Springer Series in Material Science (Springer, 2007).
5. T. T. Alkeskjold, M. Laurila, J. Weirich, M. M. Johansen, C. B. Olausson, O. Lumholt, D. Noordegraaf, M. D. Maack, and C. Jakobsen, "Photonic crystal fiber amplifiers for high power ultrafast fiber lasers," Nanophotonics **2**, 369–381 (2013).
6. F. Stutzki, F. Jansen, T. Eidam, A. Steinmetz, C. Jauregui, J. Limpert, and A. Tünnermann, "High average power large-pitch fiber amplifier with robust single-mode operation," Opt. Lett. **36**, 689–691 (2011).
7. M. M. Jørgensen, S. R. Petersen, M. Laurila, J. Lægsgaard, and T. T. Alkeskjold, "Optimizing single mode robustness of the distributed modal filtering rod fiber amplifier," Opt. Express **20**, 7263–7273 (2012).
8. J. Limpert, O. Schmidt, J. Rothhardt, F. Rser, T. Schreiber, A. Tünnermann, S. Ermeneux, P. Yvernault, and F. Salin, "Extended single-mode photonic crystal fiber lasers," Opt. Express **14**, 2715–2720 (2006).
9. M. Laurila, M. Jørgensen, K. Hansen, T. Alkeskjold, J. Broeng, and J. Lægsgaard, "Distributed mode filtering rod fiber amplifier delivering 292W with improved mode stability," Opt. Express **20**, 5742–5753 (2012).
10. T. Eidam, J. Rothhardt, F. Stutzki, F. Jansen, S. Hädrich, H. Carstens, C. Jauregui, J. Limpert, and A. Tünnermann, "Fiber chirped-pulse amplification system emitting 3.8 GW peak power," Opt. Express **19**, 255–260 (2011).
11. F. Jansen, F. Stutzki, H. Otto, T. Eidam, A. Liem, C. Jauregui, J. Limpert, and A. Tünnermann, "Thermally induced waveguide changes in active fibers," Opt. Express **20**, 3997–4008 (2012).
12. F. Poli, E. Coscelli, A. Cucinotta, S. Selleri, and F. Salin, "Single-mode propagation in Yb-doped large mode area fibers with reduced cladding symmetry," IEEE Photon. Technol. Lett. **26**, 2454–2457 (2014).

#239755 Received 24 Apr 2015; revised 19 Jun 2015; accepted 23 Jun 2015; published 9 Jul 2015

13. F. Stutzki, F. Jansen, H. Otto, C. Jauregui, J. Limpert, and A. Tünnermann, "Designing advanced very-large-mode-area fibers for power scaling of fiber-laser systems," Optica **1**, 233–242 (2014).
14. E. Coscelli, F. Poli, T. T. Alkeskjold, M. M. Jorgensen, L. Leick, J. Broeng, A. Cucinotta, and S. Selleri, "Thermal effects on the single-mode regime of distributed modal filtering rod fiber," J. Lightwave Technol. **30**(22), 3494–3499 (2012).
15. E. Coscelli and A. Cucinotta, "Modeling thermo-optic effect in large mode area double cladding photonic crystal fibers," Int. J. Mod. Phys. B **28**(12), 1442002 (2014).
16. F. Poli, A. Cucinotta, D. Passaro, S. Selleri, J. Lægsgaard, and J. Broeng, "Single-mode regime in large-mode-area rare-earth-doped rod-type PCFs," IEEE J. Sel. Top. Quantum Electron. **15**(1), 54–60 (2009).
17. A. Cucinotta, F. Poli, and S. Selleri, "Design of erbium-doped triangular photonic-crystal-fiber-based amplifiers," IEEE Photon. Technol. Lett. **16**(9), 2027–2029 (2004).
18. E. Coscelli, F. Poli, T. T. Alkeskjold, D. Passaro, A. Cucinotta, L. Leick, J. Broeng, and S. Selleri, "Single-mode analysis of Yb-doped double-cladding distributed spectral filtering photonic crystal fibers," Opt. Express **18**(1), 27197–27204 (2010).
19. F. Poli, J. Lægsgaard, D. Passaro, A. Cucinotta, S. Selleri, and J. Broeng, "Suppression of higher-order modes by segmented core doping in rod-type photonic crystal fibers," J. Lightwave Technol. **27**(22), 4935–4942 (2009).

1. Introduction

In the last two decades a huge research effort, driven by a strong industrial interest, has led to a continuous performance enhancement of high-power fiber lasers, which currently outperform other technologies in terms of brightness, beam quality, reliability, versatility and compactness [1–3]. The photonic-crystal fiber (PCF) [4] has been one of the key-enabling technologies for this improvement [5]. Indeed, it allows to maintain the Single-Mode (SM) operation while significantly increasing the fiber mode area [6,7], thus reducing the impact of nonlinear effects, which represent the main limitation for high peak power operation of pulsed fiber lasers [8]. Nevertheless, a number of recent publications have reported severe performance degradation in fiber lasers operating at high average power related to thermal effects, whose impact strengthens with the increase of the core area [9,10]. In particular the SM regime of Yb-doped Large Mode Area (LMA) PCFs is compromised by the refractive index change induced by the quantum-defect heating, which causes the appearance, in addition to the Fundamental Mode (FM), of few Higher-Order Modes (HOMs), which are suppressed in the "cold" fiber [11, 12]. It becomes therefore mandatory to consider thermal effects for the design of Yb-doped LMA PCFs operating in SM regime, suitable to provide a further fiber laser power scaling [13–15].

In this paper a new tool for the thorough analysis of the changes of the Yb-doped PCF guiding properties and of their SM regime, due to the heat load generated during the amplification process, is proposed. It is based on a spatial model, which describes the propagation of the modes along the doped fiber by solving the propagation and the population rate equations [16]. The field distributions used by the spatial model are computed with a full-vector modal solver based on the Finite Element Method (FEM) [4], combined with a simple and efficient numerical model developed to evaluate the temperature distribution and the thermally-induced refractive index change on the PCF cross-section [14]. Since the proposed model is able to consider, besides the pump, the propagation of more than one mode simultaneously at the signal wavelength [16], it can show how the gain competition between FM and HOMs evolves as a consequence of the heat generation related to the amplification process. This model feature is very important to study the heat load influence on the SM operation of Yb-doped LMA PCFs, as it has been demonstrated by simulation results obtained for an amplifier based on a Large-Pitch photonic-crystal Fiber (LPF) with 80 μm core diameter, called LPF45 [11].

This paper is organized as follows. In section 2, the thermal FEM model used to calculate the field and core overlap of the amplifier modes will be described. In section 3, the properties of an Yb-doped LPF45 amplifier are analyzed for co-propagating and counter-propagating pumping. Conclusions are drawn in the final section.

#239755 Received 24 Apr 2015; revised 19 Jun 2015; accepted 23 Jun 2015; published 9 Jul 2015

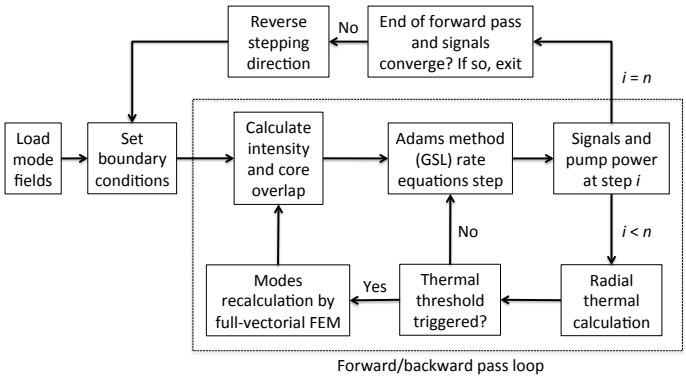

Fig. 1. Workflow of the amplifier simulator, including the full-vectorial FEM modal solver and the radial thermal model. The inner loop cycles over the fiber length divided in n steps, with the signals and pump powers updated at every length step i, while the outer loop works alternately in the forward and backward direction until convergence.

2. Thermal FEM amplifier model

The spatial model divides the fiber lengthwise in constant discrete steps, and the differential equations are assembled according to the number of propagating modes and solved at each step, using the modal field distributions to evaluate the overlap integral Γ with the doped core region S [16, 17], calculated as

$$\Gamma = \iint_S i(x,y)dxdy, \tag{1}$$

where $i(x,y)$ is the mode normalized intensity distribution [18]. The differential equations are solved by the variable-coefficient linear multistep Adams method, employing the GNU Scientific Library (GLS) implementation.

The FEM modal solver [4] calculates the guided modes using a permittivity tensor modified to account for the thermo-optic effect, which causes a local refractive index variation Δn proportional to the temperature variation ΔT. This is calculated by the thermal model [14, 15], solving the steady-state heat equation for a 1D radial heat propagation problem on an approximate fiber cross-section. The approximation consists of simplifying the fiber structure into four concentric layers (core, inner cladding, air-cladding, outer cladding) with different thermal conductivity, dissipating the heat generated in the core by conduction through the layers and final convective transfer to air or water at the outer edge of the fiber. When applied to double-clad PCFs, the model has shown accuracy comparable with FEM-based commercial software that requires much greater time and computational resources [14].

Figure 1 shows the workflow of the spatial model implementation, where the inner loop solves the step-by-step differential problem updating the signal and pump mode powers at length step i, runs the thermal model, and triggers the modes recalculation by the FEM solver upon crossing of a thermal threshold, updating the overlaps. The outer loop cycles alternately in the forward and backward direction along the fiber length divided in n steps, with properly set boundary conditions on the signals and pump input powers, until convergence is reached and the simulation ends when maximum relative signal power variation between consecutive forward passes drops to less than 10^{-6}.

The core overlap variations that the guided modes undergo under heat load have strong effect on the gain, and the simulator here presented includes for the first time, to the best of our knowl-

#239755 Received 24 Apr 2015; revised 19 Jun 2015; accepted 23 Jun 2015; published 9 Jul 2015

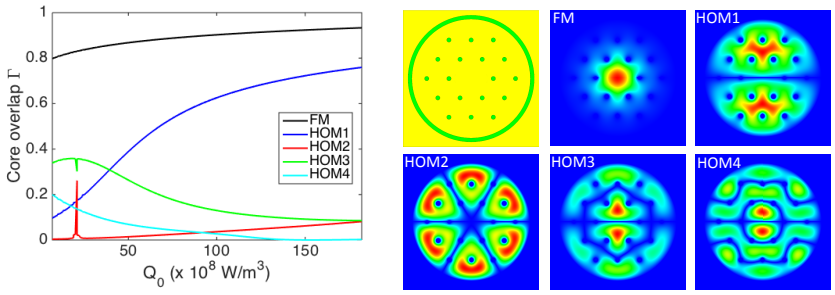

Fig. 2. FM and HOMs doped core overlap Γ for varying heat density Q_0. Notice the dispersion curves crossing with hybridization of HOM2 and HOM3 for $Q_0 = 2.1 \times 10^9$ W/m^3. On the right side, the LPF45 structure (pitch 45 μm, air-hole diameter 9 μm) and the cold-fiber magnitude of the mode magnetic field y-component H_y at 1032 nm wavelength.

edge, a full-vectorial modal solver to recalculate the mode fields under heat load and update the core overlaps as a function of length. In absence of material or radiation loss, reasonable for an air-cladding fiber, the heat density Q_0 generated on one length interval dL is attributed to the quantum defect fraction of the absorbed pump power ΔP_p:

$$Q_0 = \frac{1}{dL \cdot A_{core}} \left(1 - \frac{\lambda_p}{\lambda_s}\right) \Delta P_p, \tag{2}$$

where A_{core} is the doped core area, and λ_p and λ_s are the pump and signal wavelengths. Notice that the heat load is in general radius-dependent, however for a double-cladding fiber, the strong air-cladding pump confinement distributes it approximately uniformly across the cross-section [19], and in particular across the core, where it is uniformly absorbed. Thus, Q_0 can be written as an average heat density, mirroring the constant point-by-point core heat load.

It is indispensable to correctly track the mode fields as the effective index varies under heat load, as upon recalculation each of the modes will have a slightly different mode field, which needs to be correctly recognized and assigned to the updated power value of the same mode from the previous step. This is accomplished in either of two ways: one is to keep track of the effective index variation Δn_{eff} as a threshold to trigger the recalculation, recognizing each new mode by ranking the overlap with the same mode at the previous step. The other way is to pre-calculate a database of fields for the same mode at different Q_0 values and recalculate just the thermal profile and the permittivity tensor at each step. The database is useful in presence of mode hybridization due to dispersion curve crossings, as seen below, where the tracking of the modes as they emerge from the crossing can be problematic, and trades off greater memory occupancy for shorter calculation time.

The iterative eigenmodes-based approach is justified in this case as the non-linear thermal effect is dominated by pump absorption, signal absorption being very weak in comparison. We also considered the approximation introduced by the fiber length discretization, as the varying heat load makes the structure effectively length-variant due to the index profile change. This has been addressed in two ways, first by adjusting the index variation threshold that triggers the recalculation of the transverse modes, and secondly by adjusting the number n of length steps in which the fiber in divided. In the current case the threshold has been set to $\Delta n_{eff} = 10^{-6}$ on $n = 101$ length steps, which proved an acceptable trade-off, as recalculating the fields at every step and increasing n to 1001 steps gave output gain results within a few tenths of a dB.

For the LPF45, nine modes are propagated, that is the FM and the first 8 HOMs that are guided in proximity of the core in the cold fiber, by calculating their databases in decreasing

#239755 Received 24 Apr 2015; revised 19 Jun 2015; accepted 23 Jun 2015; published 9 Jul 2015

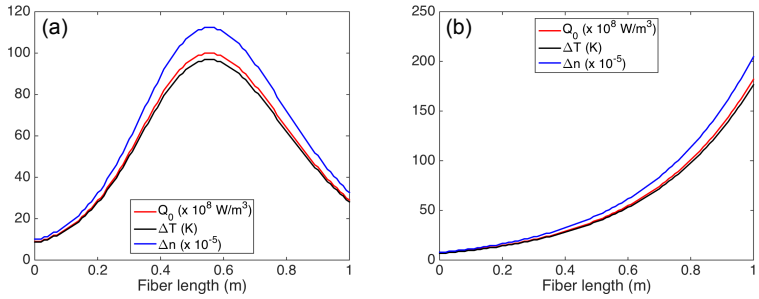

Fig. 3. Generated heat density Q_0, maximum ΔT, and maximum Δn across the fiber cross-section as a function of fiber length for (a) co-propagating pumping and (b) counter-propagating pumping ($P_p = 400$ W, $P_{FM} = 5$ W, $P_{HOM,i} = 50$ mW).

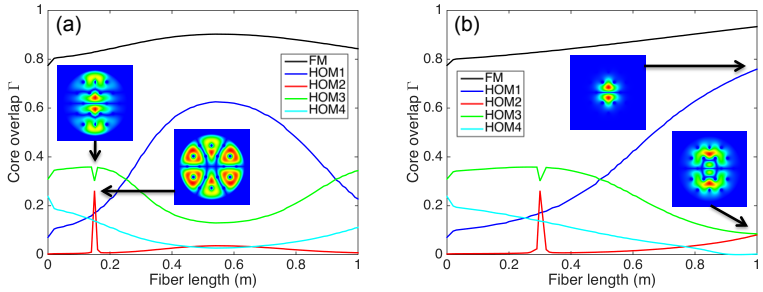

Fig. 4. FM and HOMs doped core overlap Γ vs. length for (a) co- and (b) counter-propagating pumping (same conditions as Fig. 3). Notice the field distributions in the insets.

order of cold-fiber effective index. The purpose is to investigate how modes of different cold-fiber overlap impact the amplification process as their confinement varies due to heat load. Figure 2 shows the effect of increasing heat load on the doped core overlap Γ, for the FM and the four HOMs having greater impact on amplification. Notice that the HOMs, especially the first and second, have low core confinement in the cold fiber, spreading across the inner cladding. The other HOMs are not presented here, as their low overlap did not show relevant effects on the FM amplification and kept their gain below 1 dB.

Two main effects are shown: firstly, while the confinement of FM, HOM1, and HOM2 increases with heat load, for the other modes the overlap decreases or is stationary, so they affect the FM gain less as the fiber heats up. Secondly, when mode pairs have very different overlap, but close effective index, the dispersion curves can cross as heat load increases, as seen in the overlap plot in Fig. 2, resulting in a hybrid mode; for $Q_0 = 2.1 \times 10^9$ W/m^3, HOM2 and HOM3 hybridize, and the overlap of HOM2 increases dramatically. If the slope of the dispersion curves as a function of heat load were favourable to the phenomenon, the two modes could remain hybridized, and the resulting hybrid mode could benefit from higher gain than predictable from analysis at constant Q_0.

3. Results

The amplifier modeled is made of a 1 m length of Yb-doped rod-type LPF45 fiber, considering both the co- and counter-propagating pumping configurations. The pump power at $\lambda_p = 976$ nm was $P_p = 400$ W, and the amplifier was fed an input signal at $\lambda_s = 1032$ nm whose power was split between the FM ($P_{FM} = 5$ W) and the HOMs ($P_{HOM,i} = 50$ mW). These parameters

#239755 Received 24 Apr 2015; revised 19 Jun 2015; accepted 23 Jun 2015; published 9 Jul 2015

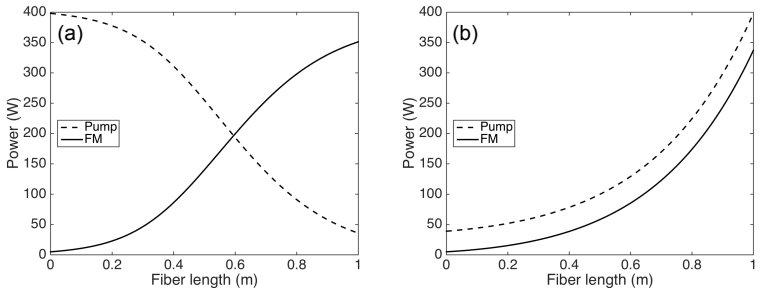

Fig. 5. Pump and FM power as a function of fiber length for (a) co-propagating pumping and (b) counter-propagating pumping (same conditions as Fig. 3).

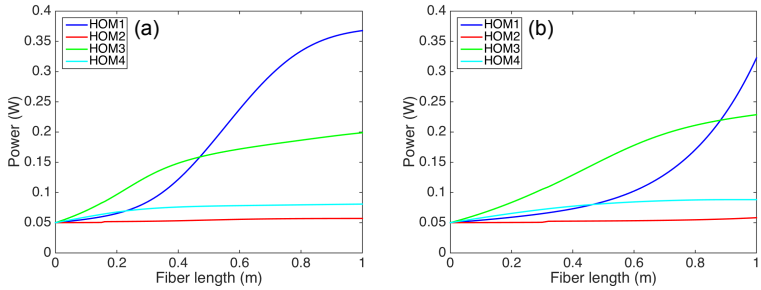

Fig. 6. HOMs power as a function of fiber length for (a) co-propagating pumping and (b) counter-propagating pumping (same conditions as Fig. 3).

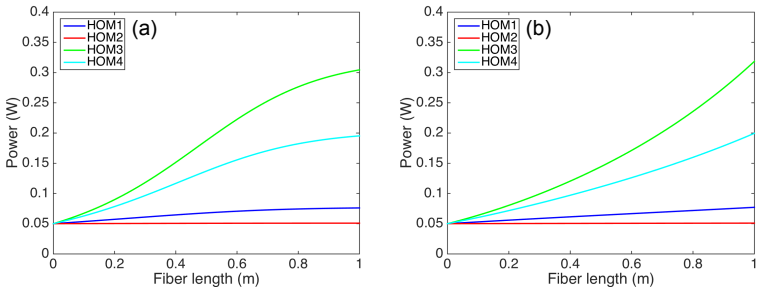

Fig. 7. HOMs power as a function of fiber length for (a) co-propagating pumping and (b) counter-propagating pumping (without thermal effects).

are representative of high-power amplifiers in use for rod-type industrial lasers [6, 9, 19]. A high pump power is employed to achieve sufficient core absorption to emphasize the different performance with and without thermal effect.

Figure 3 shows the evolution of the heat density Q_0, the maximum ΔT, and the maximum Δn across the fiber cross-section. The three quantities are proportional to each other, and the effective indices of the modes vary linearly with Q_0, which makes mode tracking easier. The counter-propagating configuration shows the highest Q_0, as pump absorption is maximum at the end, while for the co-propagating case, absorption is maximum in the middle.

Figure 4 shows the evolution of the doped core overlap Γ, where the co-propagating case shows a crossing between HOM2 and HOM3, which locally increases the normally negligible HOM2 overlap due to the hybridization. The same happens in the counter-propagating case,

#239755 Received 24 Apr 2015; revised 19 Jun 2015; accepted 23 Jun 2015; published 9 Jul 2015

where the higher Q_0 at fiber end increases overlap where the pump is strongest. Also for the other modes, there is a balancing between the higher (or lower) overlaps reached for counter-propagating pump for a shorter end span, with the less extreme overlap variations for the co-propagating pump, over a longer fiber span around the center.

Figure 5 shows the evolution of the pump and FM powers, while the HOMs are described in Fig. 6. Notice that for co-propagating pumping, HOM1 has higher gain at the center, while HOM3 has it at the start and the end, while in the other case HOM1 is lower for most of the fiber, compensating at the end with a much higher overlap. Despite the quite different power evolution, the signal gains are remarkably similar. In fact, for co-propagating pumping, the FM and HOM1 to HOM4 gains are 18.5, 8.7, 0.6, 6.0, 2.1 dB, respectively. For counter-propagating pumping, they are 18.3, 8.1, 0.7, 6.6, and 2.5 dB, respectively.

The insight provided by the model is apparent as HOM1, whose overlap is lower than 0.1 in the cold fiber, increases up to over 0.6 in the co-propagating case and over 0.7 in the counter-propagating one, breaking the single-mode regime and reaching an overall gain just 10 dB lower than the FM, despite having an input power 20 dB lower. The HOMs power $P_{HOM,i}$ was subsequently increased up to 500 mW and the simulation gave similar gain results which are not reported here. HOM1 clearly surpasses HOM3 as the most detrimental mode in the fiber under severe heat load.

For the sake of comparison, we include the HOM results for the same amplifier without thermal effects, as shown in the power curves versus length in Fig. 7. Also in this case, the signal gains are similar in both cases, however the modal makeup is totally different, since HOM3 and HOM4 have greater prominence and HOM1 is almost negligible. In fact, for co-propagating pumping, the FM and HOM1 to HOM4 gains are 18.4, 1.8, 0.07, 7.8, 5.9 dB, respectively. For counter-propagating pumping, they are 18.2, 1.9, 0.08, 8.0, and 6.0 dB, respectively. We notice that while HOM3 is significantly affected by the thermal effects, the main thermal-driven gain competition in this amplifier is between HOM1 and HOM4, which may be considered marginal at low pump powers, due to their low cold-fiber core overlap.

Recently, the first high-power amplifier with a two-ring LPF design has been demonstrated [6] on a 30 μm pitch fiber with A_{eff} =3100 μm^2, obtaining an average output power of 294 W with a mode field diameter of 62 μm in a pulsed input configuration, without showing thermally-driven instabilities. The model introduced here confirms that this fiber design can push the envelope for thermal instabilities, and is a useful tool to improve the performance limits of fiber amplifiers.

4. Conclusion

We addressed the issue of thermal effects on the single-mode regime and gain competition that affects the deployment of active double-clad large-mode-area photonic-crystal fibers to allow high power with high beam quality in fiber lasers.

The propagation of light in the fiber is modeled by solving the amplifier rate equations along the fiber segments, and the thermally-driven refractive index change is given by solving the steady-state heat equation on the fiber cross-section, with a heat load given by quantum defect fraction of the absorbed pump power. The simulator models gain competition by length-varying mode field recalculation through an embedded full-vector FEM solver.

Severe heat load is shown to affect the single-mode regime significantly, due to thermally-driven core overlap increase of modes normally spread out in the PCF cladding. Gain competition is shown between HOMs with reversed amplification capability at high heat load. Also, due to large heat-driven refractive index variations, the modal dispersion curves can cross and cause modes to suffer local degeneracy along the fiber.

#239755 Received 24 Apr 2015; revised 19 Jun 2015; accepted 23 Jun 2015; published 9 Jul 2015